HEFAT2012
9th International Conference on Heat Transfer, Fluid Mechanics and Thermodynamics
16 – 18 July 2012
Malta

FORMATION MECHANISM AND CHARACTERISTICS OF MICROLAYER IN MICRO-GAP BOILING SYSTEM

Yaohua Zhang[1]* and Yoshio Utaka[2]
*Author for correspondence
[1].Graduate school of Engineering, Yokohama National University,Yokohama,Japan
[2].Faculty of Engineering,Yokohama National Univeristy,Yokohama,Japan

E-mail: zhang-yaohua-cf@ynu.jp

ABSTRACT

Experiments were performed using laser extinction method to measure the thickness of the liquid layer formed by growing flattened bubbles between two parallel plates for gap sizes of 0.5, 0.3, and 0.15 mm. Water, toluene , ethanol and HFE7200 were used as the test fluid. A high-speed camera was used to simultaneously measure the bubble growth process and determine the bubble forefront velocity. Vapour bubbles that are generated by boiling in the present mini-gap grows exponentially due to the rapid evaporation of the thin liquid layer, which, in contrast to the steady situations considered previously, makes the phenomena highly transient. Based on the experimental data (together with the previous results for water and toluene) and scaling arguments, a non-dimensional correlation in terms of capillary number and Bond number is proposed.

INTRODUCTION

Boiling in mini/micro-scale channels is becoming increasingly important in various applications, because this technique is capable of removing large amounts of heat over small areas. For example, in order to realize fast response and compactness for a fuel cell vehicle with a reformer, the use of a microchannel type vapor generator composed of parallel plates is one possible approach to satisfy the requirements of high-efficiency heat exchange and low heat capacity. However, phase-change heat transfer mechanisms and characteristics at the micro - scale are distinctly different from those at the macro-scale. In microchannels, bubbles nucleate and quickly grow to the channel size such that elongated bubbles that are confined by the channel walls are formed, and these bubbles grow very quickly in length with a dynamic tip, which is referred to as the forefront of the bubble. The curvature of the interface between the bubble and the liquid at forefront region is clearly greater than zero, and a microlayer is simultaneously formed between the bubbles and inner heating plate walls after the dynamic tip of bubble, as shown in Fig.2. The bubble inside the microchannel is confined such that the tip is an extremely small part of the bubble, whereas most of the bubble is surrounded by a microlayer that is approximately parallel to the heating plate. In addition, as the fluid system becomes progressively smaller, the relative importance of surface tension increases. Moreover, the bulk liquid, superheated microlayers, and vapour bubbles in the microchannel affect each other in complex ways. The transient evaporation of the microlayer elongated bubbles is considered to be a major heat transfer mechanism. As such, the microlayer formed by the movement of the vapour-liquid interface has been investigated theoretically and experimentally in numerous studies.

Taylor [1] conducted experiments on a glass tube (diameter: 2 to 3 mm) filled with a glycerin-water solution that could be varied to cover a wide range of capillary number and measured the amount of liquid remaining on the tube wall after an air bubble propagated through the glass tube. The thickness of the film deposited on the wall by the propagating bubble was demonstrated to increase with an increase in capillary number. Bretherton [2] theoretically derived a prediction method for the microlayer thickness based on a lubrication approximation for the limit of Re << 1, while neglecting gravitational forces. Bretherton suggested that the liquid layer thickness could scale with capillary number. Katto and Yokoya [3] measured the temperature of a heating surface attached to the base of a water pool and the microlayer thickness under a growing flattened bubble in a narrow gap of less than 2.5 mm. They classified the boiling patterns into three regimes, and in the second pattern the formation of a microlayer, which led to heat transfer enhancement, was confirmed. Moriyama and Inoue [4], reported that the microlayer thickness follows one of two trends as the interface travelling velocity increases. They considered that a transition in the controlling mechanism occurred in the range of their experimental conditions. Two regimes for microlayer formation in their experimental study were identified according to whether the Bond number, $Bo = \frac{\rho D_i^2}{\sigma}(\frac{U^2}{2D})$ (which is calculated using the approximately

constant acceleration of interface movement rather than gravity) is greater than 2 as Eq. (1),

$$\frac{\delta}{s}=\begin{cases}0.07Ca^{0.41} & (Bo\le 2)\\ 0.10\left[\dfrac{1}{s}\sqrt{\dfrac{\mu_L t_g}{\rho_L}}\right]^{0.84} & (Bo>2)\end{cases} \quad (1)$$

where s is the distance between the two parallel plates; D is the distance from bubble forefront to incipit site; Ca is capillary number defined as $Ca=\dfrac{\mu_L U}{\sigma}$; t_g is bubble growth time; μ_L and ρ_L is viscosity and density of liquid, respectively.

For small *Bo*, the dependence of δ/s only on *Ca* suggests that the steady-flow correlation with negligible inertia should apply, whereas the microlayer formation is controlled by the viscous boundary layer when the *Bo* is greater than 2.

Tasaki and Utaka [5] measured the boiling curves for water in mini/micro channels formed between two parallel quartz glass plates with a titanium oxide-coated surface. The curves almost can be divided into a microlayer evaporation region and dryout region. In the microlayer evaporation region, heat transfer was enhanced due to the formation and sustaining of a microlayer on the heating plate with a highly wetting surface in a smaller superheat region within 3 ℃. Since the microlayer evaporation region occupied approximately 70% to 80% of the maximum heat flux, it was shown that the microlayer evaporation was the dominant heat transfer mode in microchannels. As a continuing study to Tasaki and Utaka [5], Utaka et.al [6] divided the bubble generation cycle into microlayer period and liquid saturation period. The changes in the microlayer thickness and the transition of the degree of superheat on the heat transfer surface in the microlayer period, and the temperature changes of bulk liquid in the liquid saturation period were calculated at different heat flux for gap sizes of 0.5 and 0.25mm with the assumption of one dimensional transient heat conduction in the liquid. The calculated values agreed well with the experimental results, which confirmed that the heat transfer is enhanced due to the microlayer evaporation.

Using a laser focus displacement meter, Han and Shikazono [7] measured the thicknesses of microlayer formed slug flows under an adiabatic steady condition in Pyrex glass tubes of 0.3, 0.5, 0.7, 1.0, and 1.3 mm in diameter. Ethanol, water, and FC-40 were used as test fluids. Based on the scaling analysis and numerical simulation results for the effect of Reynolds number, they assumed that the effect of inertia force could be expressed by adding a function of Reynolds number and capillary number to the curvature. Finally, using least linear square method, their experimental data was correlated as follows:

$$\frac{\delta}{D_i}=\begin{cases}\dfrac{0.67Ca^{2/3}}{1+3.13Ca^{2/3}+0.504Ca^{0.672}Re^{0.589}-0.352We^{0.629}} & (\mathrm{Re}<2000)\\ 106.0\left(\dfrac{\mu^2}{\rho\sigma}\dfrac{1}{D_i}\right)^{\frac{2}{3}} & \\ \dfrac{}{1+497.0\left(\dfrac{\mu^2}{\rho\sigma}\dfrac{1}{D_i}\right)^{\frac{2}{3}}+7330\left(\dfrac{\mu^2}{\rho\sigma}\dfrac{1}{D_i}\right)^{0.672}-5000\left(\dfrac{\mu^2}{\rho\sigma}\dfrac{1}{D_i}\right)^{0.629}} & (\mathrm{Re}>2000)\end{cases} \quad (2)$$

Under an accelerated condition [8], they assumed the bubble nose curvature to be affected by the viscous boundary layer. Based on the measured results for the microlayer thickness affected by acceleration (Han and Shikazono, [7]), a modification coefficient $f=0.692Bo^{0.414}$ was obtained by least square fitting of the data for *Bo* >1, where *Bo* is as defined in Eq. (1). Then, a correlation using Bond number, *Bo*, and capillary number for the data for *Bo* >1 is proposed as

$$\frac{\delta}{D}=\frac{0.968Ca^{2/3}Bo^{-0.414}}{1+4.838Ca^{2/3}Bo^{-0.414}} \quad (3)$$

Based on a review of the literature, a number of studies have been carried out in order to clarify the characteristics of the microlayer, most of which were performed under adiabatic conditions. However, an insufficient number of studies have

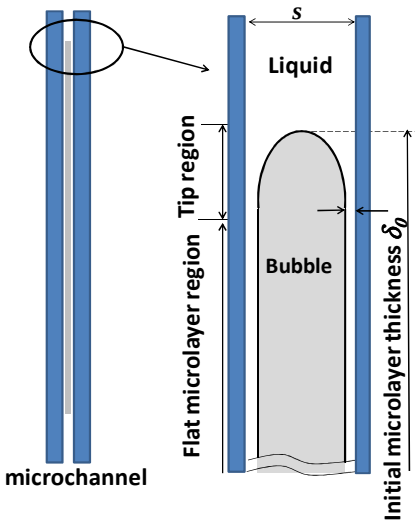

Fig.1 Schematic diagram of bubble in microchannel

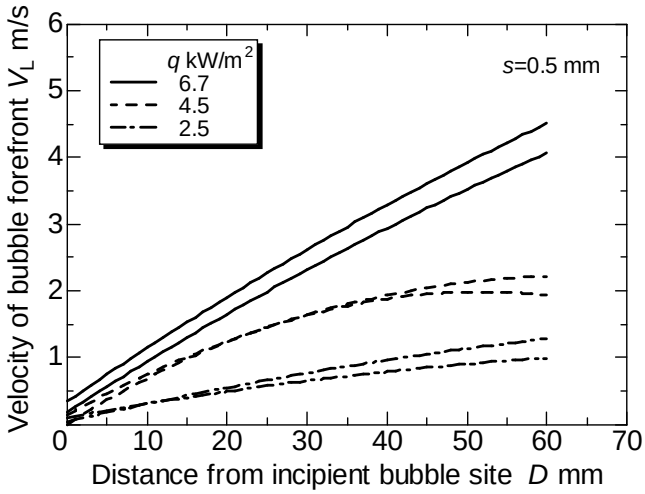

Fig.2 Velocity of bubble forefront increasing with distance from bubble site by Utaka et al., (2009)

examined the accelerated motion of bubbles confined in mini/micro channels with respect to boiling when the bubble grows nonlinearly due to rapid evaporation of microlayer (see Fig.2 by Utaka.et.al [6]). This requires the use of the full Navier – Stokes equations rather than the Stokes equations or Navier – Stokes equations that neglect local acceleration associated with unsteady flow. In the present study, in order to clarify the formation mechanism of the microlayer, a series of experiments were conducted to observe the formation and growth processes of bubbles. In addition, the initial microlayer thickness, which is defined as the thickness of the microlayer after the bubble tip at the location at which the interface between the vapour and the liquid is approximately parallel to the heating plate as shown in Fig.1, was measured directly using a laser extinction method for the HFE7200 test fluid. Furthermore, a uniform non-dimensional correlation was obtained based on the results of the experiments and the scaling argument, which provides valuable insight into the fundamental relations among system variables that are valid for different fluids under various operating conditions.

NOMENCLATURE

A	(m^{-1})	extinction coefficient
D	(mm)	distance from incipient bubble site to bubble forefront
I		laser intensity
I_0		incident laser intensity
s	(mm)	gap size
V_L	(m/s)	local bubble forefront velocity
δ	(μm)	thickness of liquid layer
δ_0	(μm)	initial thickness of microlayer
δ_{0n}		nondimensional microlayer thickness $\delta_{0n} = \delta_0 / s$
δ_V	(μm)	velocity boundary layer thickness
μ	($\mu Pa \bullet s$)	viscosity
σ	(mN/m)	surface tension coefficient
ρ	(kg/m^3)	density
Ca		Capillary number $\mu_L V_L / \sigma$
We		Weber number $\rho s V_L^2 / \sigma$
Bo		Bond number $\rho s^2 a / \sigma$
x		flow direction along the heating surface
y		direction perpendicular to the heating surface
a	m/s^2	acceleration

EXPERIMENTAL APPARATUS AND PROCEDURE

A schematic diagram of the experimental apparatus is shown in Fig. 3(a). The vapor generator is located between a He-Ne laser emitter and a Pb-Se detector. A liquid reservoir and a heating tank were placed upstream in the microchannel test section. The cross-sectional area of the liquid reservoir was large enough to maintain a constant liquid level in the microchannel, which could ensure it was close to pool boiling in the microchannel but not flow boiling. The liquid supplied to the microchannel apparatus was boiled in a heating tank to exclude non-condensable and retain the temperature of liquid to be saturation. An orifice near the inlet of microchannel was used to restrain the fluctuation of liquid flow rate caused by the bubbles growth and collapse. Vapor generated from the microchannel vapor generator flowed through a condenser and back to the reservoir. Figure 3(b) shows the details of the microchannel test section. Quartz glass ,high transparency for infrared light, was mainly utilized for the test section to enable more accurate measurements. The channel thickness between two parallel quartz glass plates can be changed by altering the spacers. Three different gap sizes of 0.15, 0.3 and 0.5mm were adopted in the present study. And the real gap size of the microchannel, as measured with a plastic-gauge, was in the range of 0.147-0.158mm for a 0.15mm test gap size. Therefore it was confirmed that the gap size was constant and sufficiently accurate with respect to the target value as reported by Utaka et al. [6].Passages for high temperature air used as the heating source to heat the microchannel were positioned at the back and the front of the microchannel. The central part of the 82 mm-high passage, which essentially served as the heating area, was narrowed to enhance heating. The width of the passage was 45 mm. The heat flux into the microchannel was controlled by varying the air temperature. The principle of the laser extinction method was used to determine the microlayer thickness by using Lambert's law as shown in equation (4).

$$\delta = -(\frac{1}{A}) \ln(I / I_0) \tag{4}$$

where δ denotes the thickness of the liquid layer the laser travels through. In this experiment, since the bubble formed symmetrically in the microchannel, the initial microlayer thickness δ_0 cited herein is calculated as $\delta_0 = 0.5\delta$. Regarding the experiment it refers to the first signal appearing on the laser ray detector when the bubble passed through the point where the laser ray passed through the microchannel, which has been reported by Utaka et al. [6]. Here, A represents the extinction coefficient, as shown in Table 1. The light intensity at the detector when the microchannel being measured is filled with steam is denoted by I_0, and the light intensity when the microchannel is filled with both a thin liquid layer and steam is denoted by I. In order to reduce the effect due to the instability of laser emitter, the laser beam is split by the beam splitter and then the reference light intensity could be measured simultaneously. This light exinction method is sufficiently accurate for measuring the microlayer thickness on a micron scale, and a detailed investigation about its measurement precision was carried out by Utaka and Nishikawa [9] for the measurement of the thickness of thin condensates of liquid mixtures during water-ethanol Marangoni dropwise condensation. The effects of ambient temperature change, reflection of laser rays, *etc*. on the values of I_0/I were examined. As a result, the ambient temperature change was the primary factor affecting the accuracy and the measurement error of the liquid condensates was approximately ±0.3 μm.

Table 1 Extinction coefficient of the test fluids

	Water	Toluene	HFE7200	Ethanol
A (m^{-1})	5.42×10^4	3.15×10^4	1.88×10^4	1.09×10^5

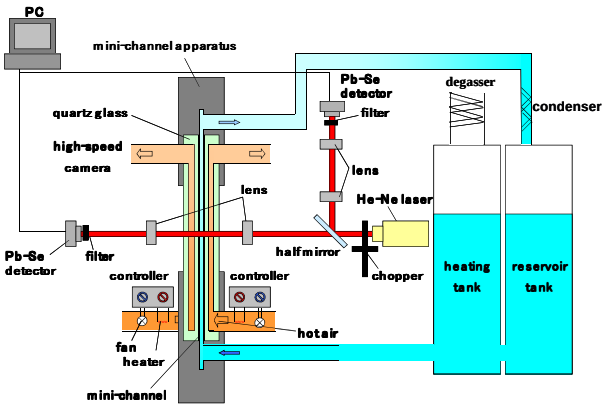

(a) Schematic of whole experimental system

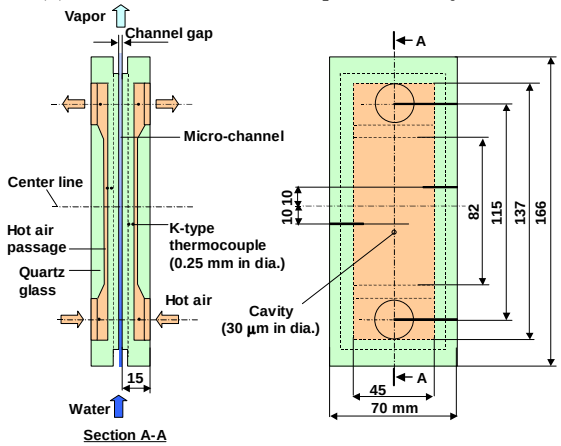

(b)Details of minichannel and heat transfer plate

Fig. 3 Experimental apparatus for measuring microlayer thickness.

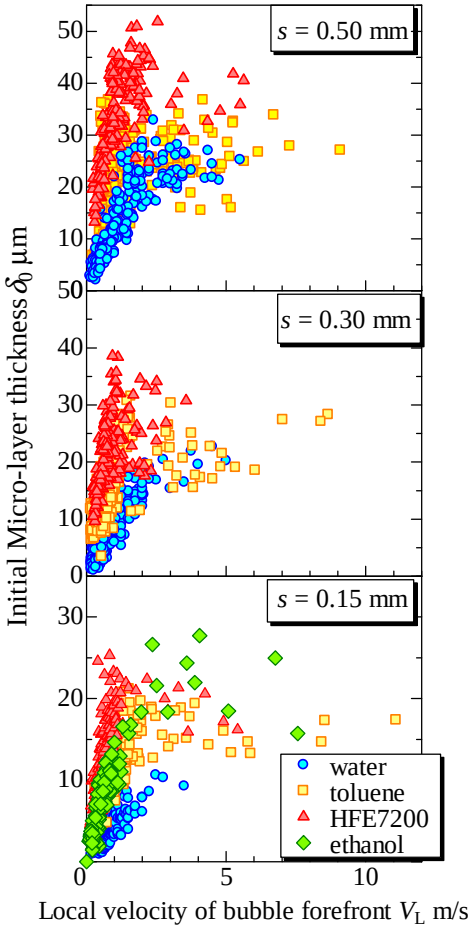

Fig. 4 Microlayer thicknesses versus local bubble forefront velocity for water, toluene and HFE7200.

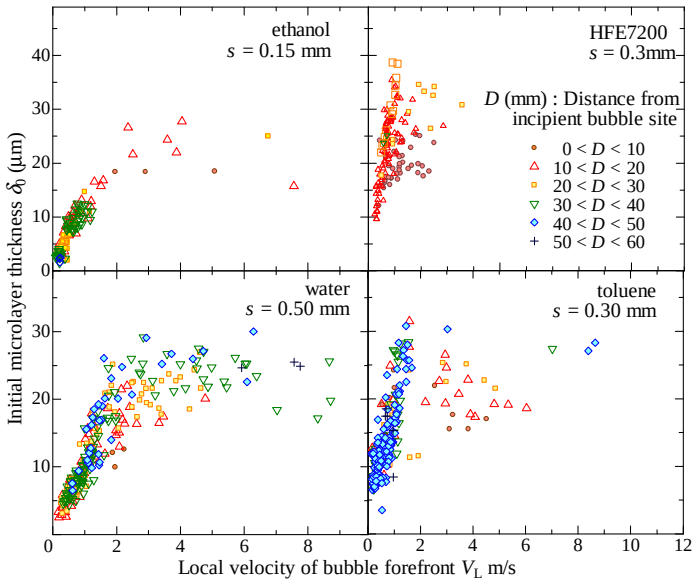

Fig.5Effect of distance from incipient bubble site *D*

RESULTS AND DISCUSSION

The microlayer forms as a result of liquid remaining on the heating surface immediately after the liquid is pushed away by the bubble growth. The microlayer thickness varies due to the effects of bubble growth rate. In the present study, attention was focused on the initial microlayer thickness δ_0, which determines the basic characteristics of heat transfer in the microchannel. The variation of the initial microlayer thickness versus the bubble forefront velocity is shown in Fig. 4 for water, ethanol, toluene and HFE7200, for three different microchannel gap sizes of 0.5, 0.3, and 0.15 mm. The initial microlayer thickness was strongly affected by the gap size, and it increased with increasing gap size. For ethanol, there was no result in the present study on gap size, except for the minimum size of 0.15 mm. This was because of the large extinction coefficient for the laser used in the present experiment. Moreover, the results for any of four liquids showed a similar tendency for any size of gap. That is, in low velocity regions, the microlayer thickness increases with forefront velocity; however, as velocity increases, the thickness becomes almost constant or decreases slightly for sufficiently high bubble forefront velocities.

Figure 5 shows, for the four kinds of liquid with representative gap size, the variations of bubble forefront velocity against the microlayer thickness with *D* (distance from bubble incipient site) as a parameter. It could be observed that in the region of high velocity, the initial microlayer thickness increases with increasing *D*, whereas in the region of low velocity the effect of *D* became weak or vanish. Instead of the Navier equation (which was used to describe the microlayer formation under an adiabatic slow flow condition, while neglecting the convectional term) or the steady Navier-Stokes equation (which was used for the adiabatic fast flow condition while considering the inertia term), the unsteady liquid motion is described by the following Navier - Stokes equations while neglecting the flow in the direction perpendicular to the heating surface:

$$\rho\frac{\partial U}{\partial t}+\rho U\frac{\partial U}{\partial x}=-\frac{\partial P}{\partial x}+\mu\frac{\partial^2 U}{\partial y^2} \tag{5}$$

The velocity gradient in flow direction can be scaled as:

$$\frac{\partial U}{\partial x}\sim\frac{V_L}{s/2} \tag{6}$$

where V_L is the local bubble forefront velocity; and unsteady term can be scaled as average acceleration. Then the left side of Eq. (5) can be scaled approximately as

$$\rho\frac{\partial U}{\partial t}+\rho U\frac{\partial U}{\partial x}\sim\rho a+\rho\frac{V_L^2}{s/2} \tag{7}$$

As shown in Fig.6, for the flat microlayer region the microlayer thickness just changes by few micrometers over several millimetres in direction of flow, therefore the gradient of microlayer thickness in flow direction could be neglected. The curvature of vapour-liquid interface may be regarded as approximately zero for the flat microlayer region, whereas the curvature increases abruptly from zero to 2/*s* near the tip region. Moreover, due to the pressure of vapour may be approximately regarded as the same in the direction of flow, the pressure gradient in microlayer near the bubble forefront can be scaled approximately as Eq. (8)

$$-\frac{\partial P}{\partial x}\sim\frac{4\sigma}{s^2} \tag{8}$$

The order of viscous term in Eq. (5) can be scaled approximately as Eq. (9), and then the Eq. (5) can be scaled as Eq. (10).

$$\mu\frac{\partial^2 U}{\partial y^2}\sim\mu\frac{V_L}{{\delta_0}^2} \tag{9}$$

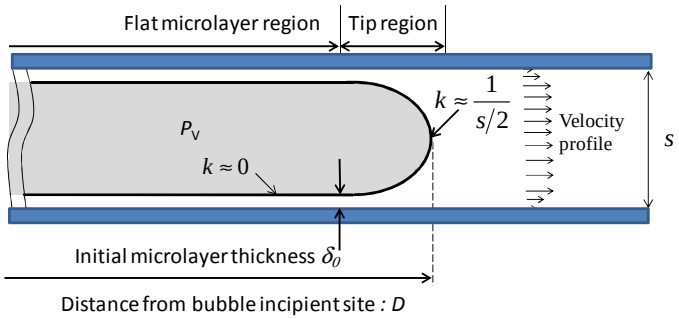

Fig. 6 Schematic diagram of bubble forefront in microchannel

$$\rho a+\rho\frac{2V_L^2}{s}\sim\frac{4\sigma}{s^2}-\mu\frac{V_L}{\delta_0^2} \tag{10}$$

Then (10) yields the following expression for the thickness:

$$\frac{\delta^2}{s^2}\sim\frac{Ca}{4-2We-Bo} \tag{11}$$

where $Bo=\frac{\rho a s^2}{\sigma}$ is Bond number that represents the ratio of the inertial force due to acceleration to the surface tension force; $We = \rho u^2 s/\sigma$ is Weber number that represents the ratio of the inertial force to the surface tension force. Equation (11) reveals that the nondimensional microlayer can be described by the nondimensional groups of *Ca*, *We*, and *Bo*. However, the derivation of an accurate prediction equation directly from Eq. (11) and experimental data is quite difficult.

In order to create a better correlation, a trial has been done by nondimension analysis as following. Based on the experiment it has been understood that the microlayer thickness is related as

$$\delta_0\sim f(V_L,D,s,\rho,\mu,\sigma) \tag{12}$$

The experiment and simulation results shown the microlayer thickness is proportional with viscosity and density, and inversely proportional with surface tension. Therefore the thickness can be related as

$$\delta_0\sim\frac{\mu\rho}{\sigma}\sim\frac{\mathrm{M\tau}}{\mathrm{L}^4} \tag{13}$$

By introducing the V_L and *s* to which the microlayer thickness is also proportional due to the experiment results, the right side of Eq. (13) can be nondimensionalized as

$$\frac{\rho\mu{V_L}^3 s}{\sigma^2}\sim 1 \tag{14}$$

Due to the π theory, we can also derive that the nondimensional microlayer thickness is qualitatively a function of *Ca*, We and Bo as shown in Eq. (15) like scaling analysis result. Here, according to the study of Moriyama and Inoue (1996), as velocity increases the microlayer is limited by the viscous boundary layer. Therefore, perhaps it is a good choice to nondimensionalize the microlayer thickness with viscous boundary layer thickness, and then the nondimensional relationship is changed to be

$$\frac{\delta_0}{\delta_V} \sim \frac{\rho\mu V_L{}^3 s}{\sigma^2} = Ca \cdot We \tag{15}$$

All of the experiment data is plotted in Fig. 7, where the coordinate is the nondimensional groups of Eq. (14). It shows that each of fluid correlated well without apparent discord.

$$\frac{\delta_0}{\delta_V} = 0.48\left(\frac{\rho\mu V_L{}^3 s}{\sigma^2}\right)^{0.45} \tag{16}$$

$$\frac{\delta_0}{\delta_V} = 0.619\left(\frac{\rho\mu V_L{}^3 s}{\sigma^2}\right)^{0.03} \tag{17}$$

Equations (16) and (17) are fitting equations for experiment data with $\rho\mu V_L{}^3 s/\sigma^2 < 0.1$ and $\rho\mu V_L{}^3 s/\sigma^2 > 10$ plotted as solid line in Fig. 7, and the region between the two regions is considered as the transition region. Then the continuous equation can be created by combining the two equations obtained from Fig.7 as shown in Eq. (18) (dash line in Fig. 7).

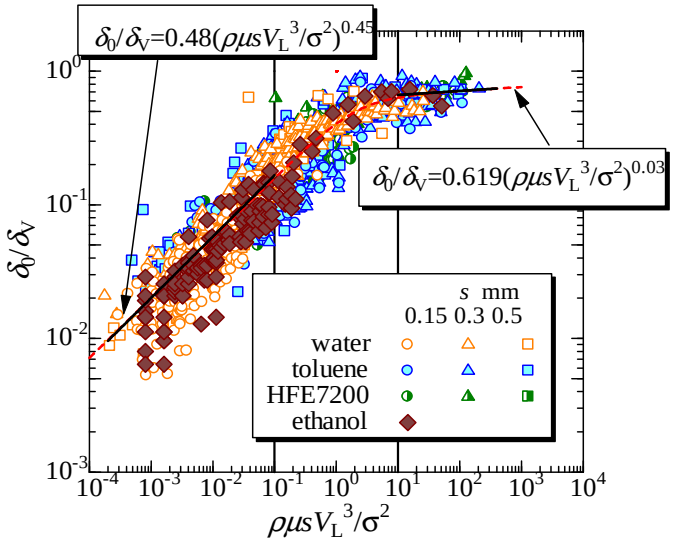

Fig. 7 Microlayer thickness nondimensionalized by viscous boundary layer versus dimensional group of $\rho\mu V_L{}^3 s/\sigma^2$

$$\frac{\delta_0}{\delta_V} = \left\{[0.48(\frac{\rho\mu V_L{}^3 s}{\sigma^2})^{0.45}]^{-8} + [0.619(\frac{\rho\mu V_L{}^3 s}{\sigma^2})^{0.03}]^{-8}\right\}^{-1/8} \tag{18}$$

Here, although in low velocity region formation of a thin liquid film is considered not to be dependent strongly on boundary layer, it is thought that the influence of force of inertia and acceleration in addition to viscosity and surface tension as for thin liquid film thickness formation should be considered. It will be found that the effect of acceleration, surface tension and viscosity are included in the left side of Eq. (16) and (17). If the boundary layer thickness is transformed as

$$\delta_{Vn} = \frac{\delta_V}{s} = \sqrt{\frac{\mu D}{\rho V_L s^2}} = \sqrt{\frac{2D\sigma}{\rho V_L{}^2 s^2} \cdot \frac{\mu V_L}{2\sigma}} = \sqrt{\frac{1}{2}} Ca^{0.5} Bo^{-0.5} \tag{19}$$

Then, Eq. (19) can be rewritten as a combination of *Ca*, *We* and *Bo* as Eq. (21).

$$\frac{\delta_0}{s} = \begin{Bmatrix}[0.34 Ca^{0.95} We^{0.45} Bo^{-0.5}]^{-8} + \\ [0.43 Ca^{0.53} We^{0.03} Bo^{-0.5}]^{-8}\end{Bmatrix}^{-1/8} \tag{20}$$

In order to confirm the accuracy of Eq. (20) in detail, the experiment data was firstly divided into several groups based on the certain range of Weber number, secondly the data with fixed range of *We* was divided into subgroups based on corresponding range of Bond number. The correlation of Eq. (20) was plotted in Fig.8(a-j). And the correlations based on upper and lower boundary value of *We* are plotted in dash and solid lines in red or back corresponding with the boundary value of *Bo*. It is found that the experiment data in each range of Weber number and Bond number is shown relative good agreement with the correlation of Eq. (20) derived from dimension analysis.

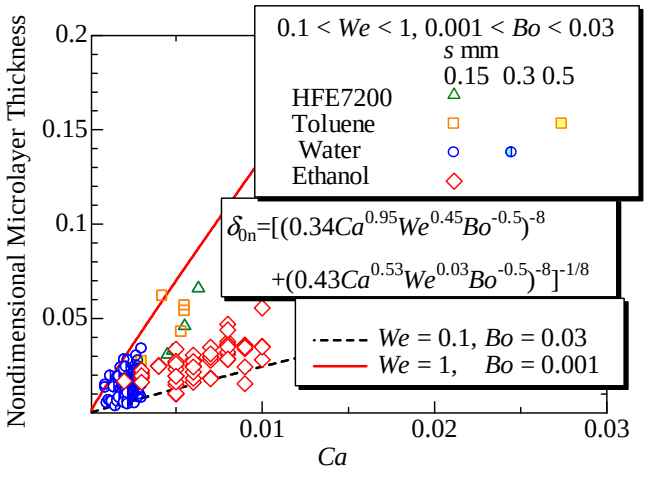

(a)

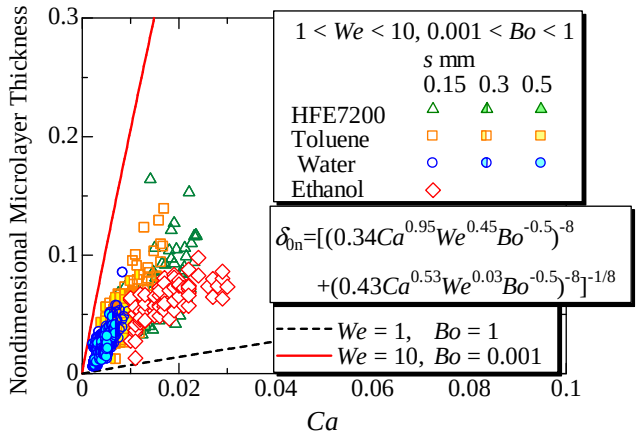
1 < We < 10, 0.001 < Bo < 1
s mm
0.15 0.3 0.5
HFE7200
Toluene
Water
Ethanol
δ0n=[(0.34Ca^0.95We^0.45Bo^-0.5)^-8
+(0.43Ca^0.53We^0.03Bo^-0.5)^-8]^-1/8
We = 1, Bo = 1
We = 10, Bo = 0.001
Nondimensional Microlayer Thickness
Ca

(b)

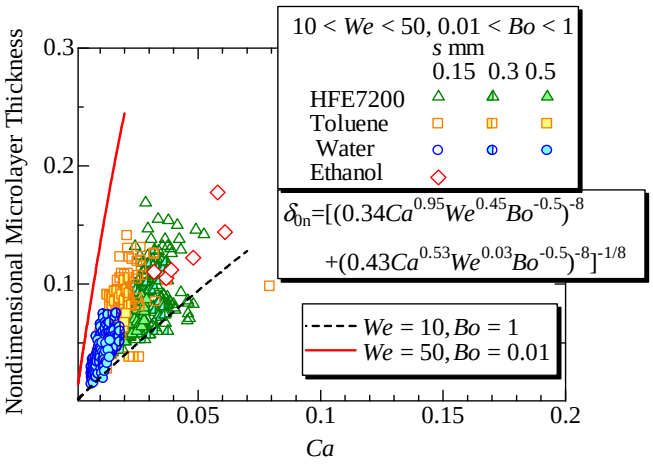
10 < We < 50, 0.01 < Bo < 1
s mm
0.15 0.3 0.5
HFE7200
Toluene
Water
Ethanol
δ0n=[(0.34Ca^0.95We^0.45Bo^-0.5)^-8
+(0.43Ca^0.53We^0.03Bo^-0.5)^-8]^-1/8
We = 10, Bo = 1
We = 50, Bo = 0.01
Nondimensional Microlayer Thickness
Ca

(c)

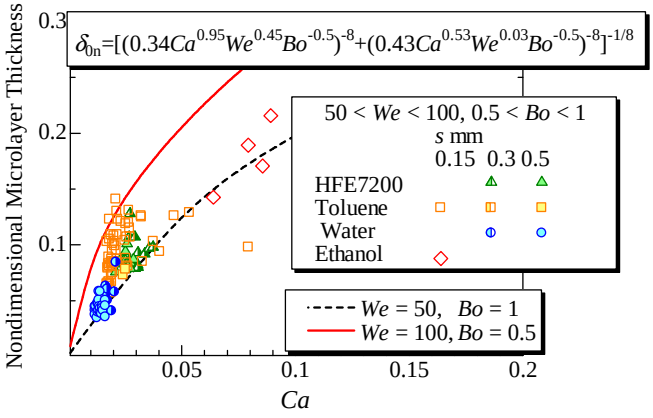
δ0n=[(0.34Ca^0.95We^0.45Bo^-0.5)^-8+(0.43Ca^0.53We^0.03Bo^-0.5)^-8]^-1/8
50 < We < 100, 0.5 < Bo < 1
s mm
0.15 0.3 0.5
HFE7200
Toluene
Water
Ethanol
We = 50, Bo = 1
We = 100, Bo = 0.5
Nondimensional Microlayer Thickness
Ca

(d)

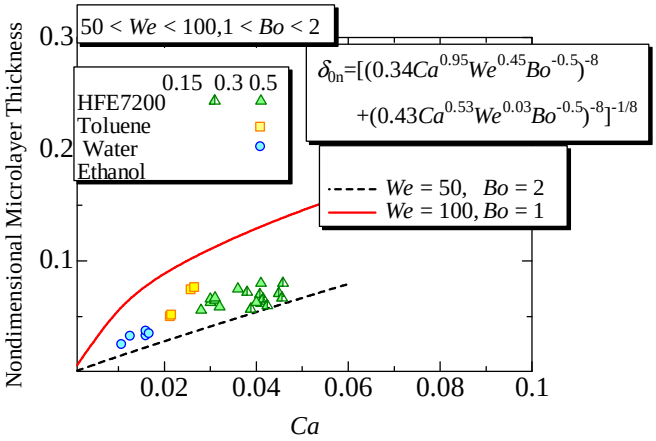
50 < We < 100,1 < Bo < 2
δ0n=[(0.34Ca^0.95We^0.45Bo^-0.5)^-8
+(0.43Ca^0.53We^0.03Bo^-0.5)^-8]^-1/8
0.15 0.3 0.5
HFE7200
Toluene
Water
Ethanol
We = 50, Bo = 2
We = 100, Bo = 1
Nondimensional Microlayer Thickness
Ca

(e)

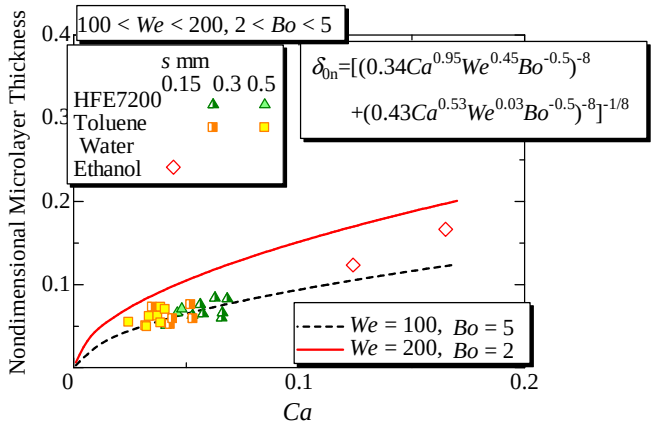
100 < We < 200, 2 < Bo < 5
s mm
0.15 0.3 0.5
HFE7200
Toluene
Water
Ethanol
δ0n=[(0.34Ca^0.95We^0.45Bo^-0.5)^-8
+(0.43Ca^0.53We^0.03Bo^-0.5)^-8]^-1/8
We = 100, Bo = 5
We = 200, Bo = 2
Nondimensional Microlayer Thickness
Ca

(f)

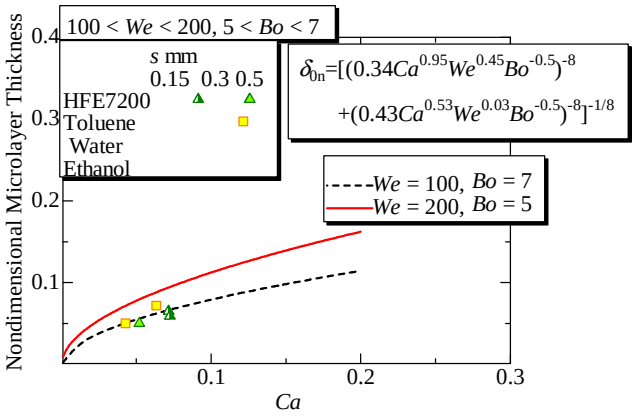
100 < We < 200, 5 < Bo < 7
s mm
0.15 0.3 0.5
HFE7200
Toluene
Water
Ethanol
δ0n=[(0.34Ca^0.95We^0.45Bo^-0.5)^-8
+(0.43Ca^0.53We^0.03Bo^-0.5)^-8]^-1/8
We = 100, Bo = 7
We = 200, Bo = 5
Nondimensional Microlayer Thickness
Ca

(g)

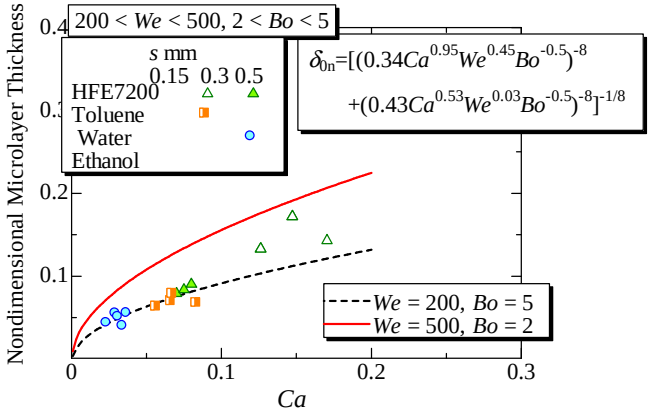

(h)

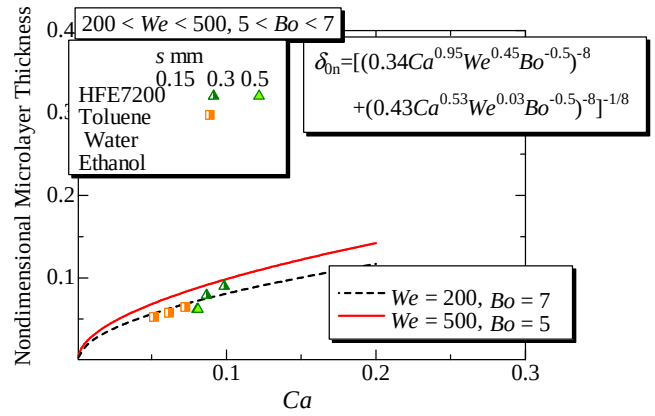

(i)

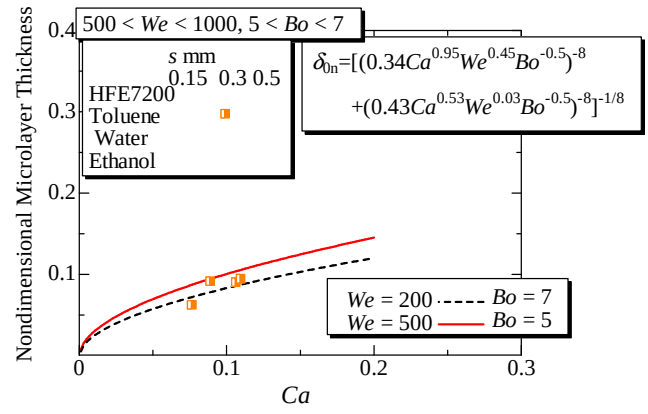

(j)

Fig. 8 Comparison between correlations and experiments

CONCLUSIONS

Experiments were performed using the laser extinction method to directly measure the microlayer that forms on a heating surface due to vapour growth during boiling in a mini/microchannel formed by two parallel pieces of quartz glass for water, ethanol, toluene and HFE7200. Based on the results of experiments and the discussion by scaling analysis and dimension analysis the following results were obtained.

(1) The initial microlayer thickness was mainly determined by the gap sizes, velocity of the bubble forefront, and the effect of distance from bubble incipient site to bubble forefront become significant with increasing of bubble velocity.

(2) Scaling analysis from full Navier-Stokes equation (with neglecting the flow in the direction perpendicular to the heating surface) showed that the microlayer formation during boiling in mini/microchannel can be described as function of capillary number, Weber number and Bond number. Based on dimension analysis, the experiment data was found to be correlated well with the group of δ_0 / δ_V and $\rho\mu V_L^3 s/\sigma^2$.

(3) Based on the results of experiments a uniform empirical correlation for the nondimensional microlayer thickness, δ_0 / s correlated in the form of *Ca*, *We* and *Bo* in mini/micro parallel channels was proposed. The present correlation predicts the experimental results within accepted error range.

REFERENCES

(1) Taylor, G.I., Deposition of a viscous fluid on the wall of a tube, *J. Fluid Mech.*, Vol.10, (1961), pp. 1161-1165.

(2) Bretherton F.P., The motion of long bubbles in tubes. *J. Fluid Mech.*, Vol.10, (1961), pp.166-188.

(3) Katto, Y., and Shoji, M., Principal mechanism of micro-liquid-layer formation on a solid surface with a growing bubble in nucleate boiling, *Int. J. Heat Mass Transfer*, Vol.13, (1970), pp. 1299-1311

(4) Moriyama, K., and Inoue, A., Thickness of the liquid film formed by a growing bubble in a narrow gap between two horizontal plates, *Trans. ASME, J. Heat Transfer*, Vol.118,(1996) ,pp.132-139.

(5) Tasaki, Y. and Utaka, Y., Effect of Wettability on Boiling Heat Transfer Characteristics in Micro-Channel Vapor Generator, *Int. J. Transport Phenomena*, Vol.5, No.4 (2003), pp.295-302

(6) Utaka, Y., Okuda, S. and Tasaki, Y., Configuration of the micro-layer and characteristics of heat transfer in a narrow gap mini/micro-channel boiling system, *International Journal of Heat and Mass Transfer*, Vol.52, (2009), pp.2205-2214.

(7) Han, Y. and Shikazono, N., Measurement of the liquid film thickness in micro tube slug flow , *Int. J. Heat and Fluid Flow*, Vol.30, No.5(2009), pp.842-853

(8) Han, Y. and Shikazono, N., The effect of bubble acceleration on the liquid film thickness in micro tubes, *Int. J. Heat and Fluid Flow*, Vol.31, (2010), pp. 630-639.

(9) Utaka, Y. and Nishikawa, T., 2003, An investigation of liquid film thickness during Solutal Marangoni condensation using laser absorption method: absorption property and examination of measuring method, *Heat Transfer-Asian Res.*Vol.30 (8) , pp. 700-711.